University of Groningen

Genesis and mechanism of microstructural scale deformation and cracking in ZnAlMg coatings

Ahmadi, Masoud; Salgin, Bekir; Kooi, Bart J.; Pei, Yutao

IMPORTANT NOTE: You are advised to consult the publisher's version (publisher's PDF) if you wish to cite from it. Please check the document version below.

Document Version
Publisher's PDF, also known as Version of record

Publication date:
2020

[Link to publication in University of Groningen/UMCG research database](#)

Genesis and mechanism of microstructural scale deformation and cracking in ZnAlMg coatings

Masoud Ahmadi [a], Bekir Salgın [b], Bart J. Kooi [c], Yutao Pei [a,*]

[a] Department of Advanced Production Engineering, Engineering and Technology Institute Groningen, Faculty of Science and Engineering, University of Groningen, Nijenborgh 4, 9747 AG Groningen, the Netherlands
[b] Tata Steel, Research & Development, P.O. Box 10000, 1970 CA IJmuiden, the Netherlands
[c] Nanostructured Materials and Interfaces, Zernike Institute for Advanced Materials, Faculty of Science and Engineering, University of Groningen, Nijenborgh 4, 9747 AG Groningen, the Netherlands

HIGHLIGHTS

- Plastic deformation-based criteria are revealed to comprehend the origin and mechanism of cracking in ZnAlMg coatings.
- Micro-mechanical properties and orientations of microstructural constituents are correlated with the cracking/damage.
- Most of the cracks were nucleated in detrimental binary eutectic phase.
- Substantial heterogeneous deformation within the coating led to stress/strain localization mostly in the binary eutectic.
- Primary zinc grains with a low Schmid factor ($m < 0.32$) and a low strain hardening exponent ($n < 0.33$) experienced cracking.

GRAPHICAL ABSTRACT
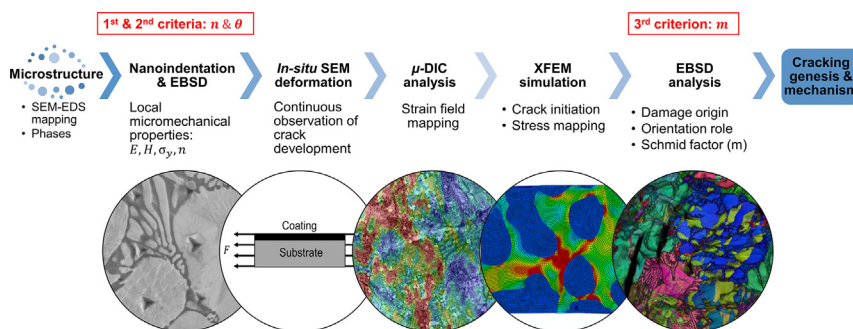
ARTICLE INFO

ABSTRACT

In-depth investigation of the microscale deformation behavior of ZnAlMg coatings is essential to reveal the origin and mechanism of cracking in these coatings. In this work anisotropic microstructural damage and cracking of multiphase Zn1.8Al1.8Mg alloy coatings produced by hot-dip galvanization process on a steel substrate have been studied extensively. Nanoindentation coupled with orientation image microscopy (OIM) is utilized to determine the local micro ductility/strength of the existing phases as well as the orientation dependent micromechanical properties of primary zinc grains. Plastic deformation and damage behavior of the coating are evaluated through in-situ tensile/bending tests, micro-digital image correlation and in-situ OIM analyses. Stress distribution fields and nucleation sites of cracks within the coating microstructure are investigated using extended finite element method. Three quantitative plastic deformation-based criteria are revealed to correlate the coating microstructure to micro-mechanical properties to comprehend the cracking phenomenon. In particular, the binary eutectic is identified as the most detrimental constituent for compatible plastic deformation. Local strain hardening exponent and Schmid factor of primary zinc grains are found to play a significant role in clarifying the cracking behavior. The results of this study are considered as an important step towards designing microstructure controlled ZnAlMg coatings with superior formability.

* Corresponding author.
E-mail address: y.pei@rug.nl (Y. Pei).

1. Introduction

Zinc-coated steels produced *via* hot-dip galvanization (HDG) process are regarded as the vital materials for household, construction and automotive industries. By addition of aluminum and magnesium (both elements >1.5 wt%) to the conventional pure zinc coatings, the resultant ZnAlMg coating offers superior corrosion resistance and friction/wear performance [1,2]. Nevertheless, these hot-dip ZnAlMg coatings currently deliver very low cracking resistance once subjected to forming processes [3,4]. Microstructural damages of ZnAlMg coatings lead to cracking in severely deformed areas and result in the formation of large opening sites and subsequently deteriorate the in-service corrosion resistance. Thus, obtaining in-depth knowledge of the underlying causes and sources of the damage is considered to be instrumental in designing cracking-resistant ZnAlMg coatings.

Most of the research works on ZnAlMg coatings in the literature have been assigned to microstructure, corrosion resistance and production techniques rather than mechanical properties, cracking behavior and forming performances [5–10]. Previous studies have examined the mechanical response and cracking of conventional hot-dip pure zinc coatings, reporting the effect of coating thickness [11], the role of texture [12], grain boundary features [13], roughness driven plasticity [14], intergranular cracking [15], adhesion performance [16], deformation modes [17], substrate and stress state roles [18,19], and HDG process parameters [20,21]. A few studies have been also conducted on the as-cast bulk alloys with chemical composition close to ZnAlMg coatings. It has been reported that, the deformation of cast ZnAlCuMg alloy is substantially influenced by temperature and strain rate, resulting in the activation of various basal, non-basal and twining systems [22]. Primary zinc (Zn) grains are declared as the most probable suppliers to bulk deformation compared to existing eutectics in ZnAl alloy [23]. A specific study regarding cracking of ZnAlMg coatings was conducted by Park et al. [24] on Zn2.5Al3Mg and Zn6Al3Mg coatings. They utilized cross-sectional electron backscatter diffraction (EBSD) analysis and stated that crystallographic orientations of the primary Zn and the eutectic constituents affect the cracking tendency of the coating subjected to bending. Based on the cross-sectional observations, they reported that the occurrence of cracking alongside the basal plane in ⟨0001⟩ perpendicular to normal direction of the zinc grains/eutectic phases was remarkably high. They stated that, due to the difference in coefficient of thermal expansion (CTE) between the coating phases and the substrate, a tensile stress regime is generated in the coating. The anisotropic elastic moduli (E) of the phases present were used to interpret cracking in the coating. In addition, they observed microstructure cracking both in the as-received and deformed conditions of some samples. Although they performed valuable observation on the cracking phenomenon of ZnAlMg coatings and indicated the effect of crystallographic orientation, there still remain many open questions and uncertainties regarding the actual cracking behavior of these coatings. In particular, the following critical issues are not sufficiently covered: (1) the micro-mechanical analysis of the phases present and their interaction in the microstructure, (2) the origin and mechanism of the microstructural scale cracking, (3) the plastic deformation-based causes to explain the orientation dependent cracking of these coatings, where it must be noted that the cracking of metallic materials is mainly governed by plastic deformation rather than by elastic behavior as received main attention in previous work. Moreover, to get proper insight in cracking behavior, it is required (1) to perform more extensive orientation imaging microscopy (OIM) with more statistical data, (2) to map with sufficient local precision stress/strain field during deformation within the microstructure to capture the onset and localization of damage and cracks. Only such extensive studies will develop the required knowhow allowing the developments of new precise strategies to reduce the cracking tendency and improve the ductility of ZnAlMg coatings.

Considering the aforementioned literature, plastic deformation and cracking mechanism of ZnAlMg coatings have thus not been systematically scrutinized yet. In this study owing to *in-situ* evaluations, we have established an in-depth approach towards comprehending the genesis and mechanism of microstructural scale cracking in Zn1.8Al1.8Mg coatings (MagiZinc®) for the first time. To address this, real-time *in-situ* scanning electron microscopy (SEM) deformation assessments, multi-aspect microstructural and OIM, local micro-mechanical properties determinations by nanoindentation, micro-digital image correlation (μ-DIC) and finite element analysis (FEA) were exploited to analyze microstructural evolution, plastic deformation and damage/cracking of ZnAlMg coatings. The main contribution of the present paper is to correlate the micro-mechanical properties and crystallographic orientations of microstructural constituents with cracking/damage behavior. In particular, we have developed quantitative plastic deformation-based criteria - as a collective predictive benchmark - to firstly comprehend damage and cracking origin/mechanism, and secondly providing some insights to enhance the cracking resistance within these coatings.

2. Materials and methods

The as-received Zn1.8Al1.8Mg coated steel sheets with a total thickness of 0.61 mm (coating thickness 10–15 μm on both sides of the steel sheets) produced by continuous hot-dip galvanization process (HDG) were cut into small samples (10 × 10 mm) for microstructural characterizations. The surface of the samples was first mechanically polished using 1 μm diamond suspension and water-free lubricant on a Struers MD Nap disc to obtain relatively smooth surface. Thereafter it was flat ion milled for 15 min by means of an ion polisher (JEOL IB-19520CCP) in order to attain a good surface quality for microstructural characterizations, nanoindentation tests and EBSD analysis. The surface morphology/microstructure of the coating was studied by scanning electron microscopy (SEM, Philips XL30-FEG ESEM). Electron dispersive X-ray spectroscopy (EDS) mapping was performed in Tescan LYRA SEM–FIB dual beam microscope.

In order to evaluate local micromechanical properties of different phases in the coating microstructure, nanoindentation experiments are conducted utilizing MTS Nano Indenter XP with a Berkovich tip using the continuous stiffness measurement (CSM) mode. Load controlled indentations with an applied force of 3 mN and spacing of 8 μm between the indents are employed. This spacing value is chosen based on the grain size of primary zinc to collect enough statistical data over the microstructural components of the coating. Yield strength (σ_y) and strain hardening exponent (n) associated with each indent are calculated using raw nanoindentation data analyzed in a MATLAB code generated based on the method proposed by Dao et al. [25].

To analyze the chronological damage and cracking mechanism in the coating, *in-situ* tensile tests were carried out utilizing Kammrath & Weiss (K&W) 5000 N tensile and compression module in SEM. The tensile samples had a gauge dimension of 11.5 mm (length) × 3.5 mm (width) × 0.61 mm (thickness). The cracking behavior was also evaluated by *in-situ* bending (buckling) experiments using the same stage on 20 mm (length) × 7 mm (width) × 0.61 mm (thickness) rectangular samples (see Fig. S1 in the supplementary data). In this study, *in-situ* bending tests were performed in such a way that two shorter sides of the rectangular samples were fixed and compressed using the module. *In-situ* μ-DIC analysis was performed to acquire strain mapping in the multi-phase microstructure of the coating. For high accuracy DIC study, the tensile sample was prepared with the same procedure given earlier and followed by decoration of the coating surface using yttria-stabilized zirconia (YSZ) nano-particles solution to achieve proper image contrast and particle distribution. GOM Correlate software was used for DIC post processing analysis. The same preparation method was also employed for tensile/bending test samples. The configuration of the *in-situ* tests and tensile specimen are provided in supplementary data (see Fig. S2a). It should be mentioned that, in this study all the mechanical tests were conducted at room temperature.

OIM analyses on nanoindented regions and cracked zones were performed using SEM, Philips XL30 ESEM equipped with EBSD detector. Scanning step size of 200 nm and acceleration voltage of 25 kV were used to acquire EBSD patterns. In order to locally investigate the orientation dependent damage and cracking initiation in the microstructure, *in-situ* OIM and tensile test were carried out utilizing a K&W tensile module in a Tescan LYRA FIB/SEM equipped with an EDAX TSL OIM system (see Fig. S2b in supplementary data for the configuration of *in-situ* EBSD experiment). All the obtained EBSD data were then analyzed by means of EDAX-TSL OIM™ Analysis 8 software. In order to determine the Schmid factor maps, principle slip systems of zinc phase *i.e.* basal, prismatic and first order pyramidal and their equivalent crystallographic families were implemented by considering the corresponding applied stress state.

Extended finite element method (XFEM) was exploited to simulate stress fields and predict the damage/crack initiation within the coating microstructure subjected to tension. For this purpose, a two dimensional (2D) microstructural representation was utilized and exposed to uniaxial tensile force from both lateral sides. The model was generated by partitioning the 2D representation in accordance with a distribution and morphology of the phases in a real region of interest (ROI) of the microstructure. The mechanical properties obtained by nanoindentation and *in-situ* tensile/DIC tests were implemented into the FEM model for the corresponding phases within the microstructure. Traction-separation damage model was used to capture the crack initiation phenomenon in this simulation executed in commercial ABAQUS™ software.

3. Results and discussions

3.1. Microstructure and local mechanical properties

SEM micrographs of Zn1.8Al1.8Mg coating microstructure are demonstrated in Fig. 1. The microstructure consists of three different constituents, *i.e.* primary zinc (Zn), binary eutectic (BE) and ternary eutectic (TE). Elemental distribution within the microstructure was revealed by EDS (see Fig. 1b–d). As it can be observed, Zn is spread all over the coating, whereas magnesium is detected in the binary and ternary eutectics. Aluminum element can be only observed in the ternary eutectic. The dark ribbons in the binary and ternary eutectics correspond to $MgZn_2$ intermetallic compound as shown in Fig. 1a. Therefore, thin binary eutectic platelets of $Zn/MgZn_2$ and fine granular/fibrous ternary eutectic composed of $Zn/MgZn_2/Al$ are surrounded by primary zinc grains (10 to 50 μm in diameter) within the typical microstructure of Zn1.8Al1.8Mg coating. It should be noticed that, the fraction of $MgZn_2$ phase in the binary eutectic is significantly higher than that of the ternary eutectic.

From solidification point of view, it has been reported that [26], first Zn crystals are solidified followed by the solidification of interdendritic binary eutectic and ternary eutectics, respectively. Depending on the coating composition and HDG processing parameters, several types of microstructures are reported in the literature [27]. Due to non-equilibrium conditions in HDG process (including fast cooling rates), it is less likely that Mg_2Zn_{11} intermetallic has been formed (see XRD pattern of the coating in Fig. S3 in supplementary data). The characteristic
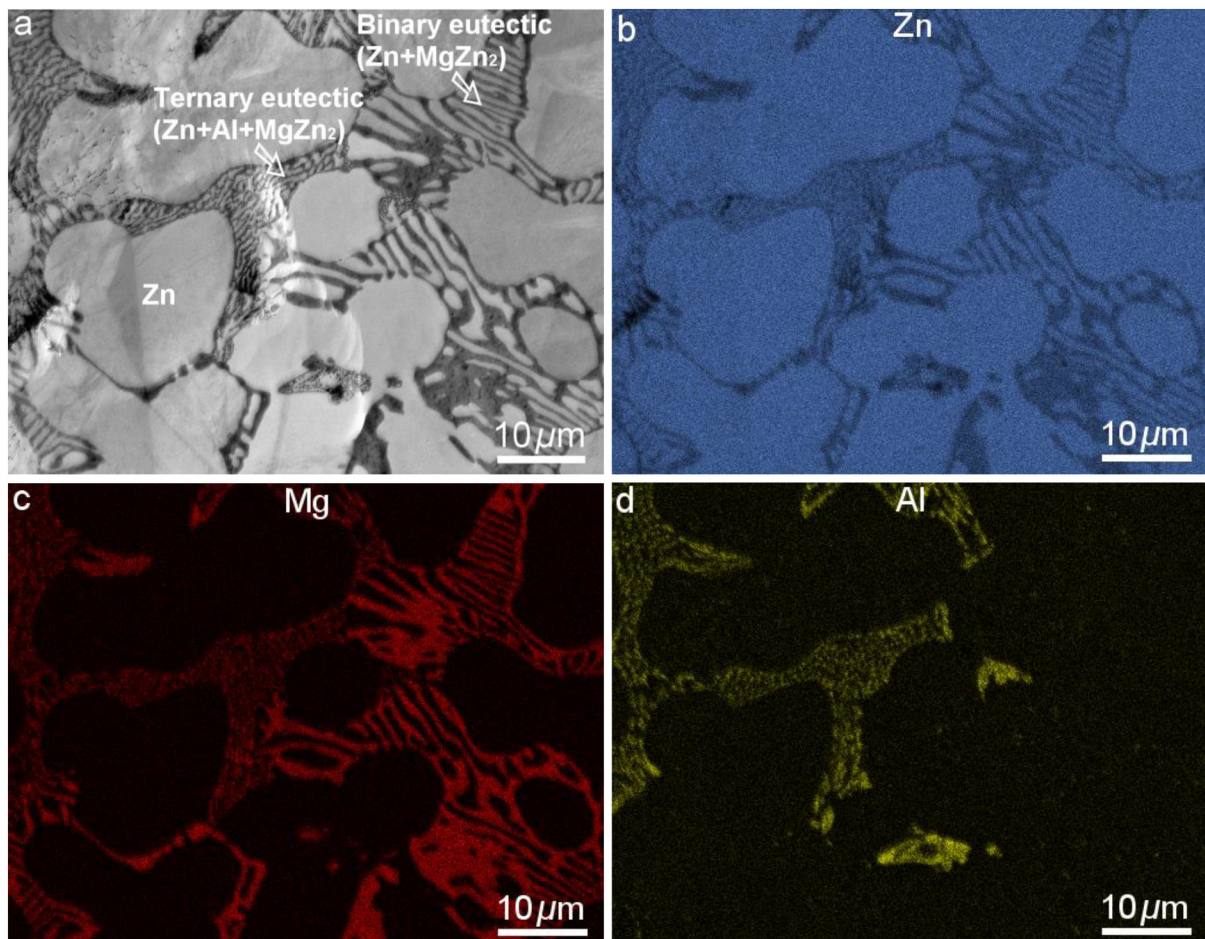

Fig. 1. (a) SEM micrograph showing the microstructure of ZnAlMg coating consisting of three phases, and the corresponding elemental map of (b) zinc, (c) magnesium and (d) aluminum.

diffraction peaks associated with Mg_2Zn_{11} phase are not detected in the obtained XRD pattern.

The first and foremost step towards understanding the mechanical response of a polycrystalline multiphase metallic material is to study the local mechanical properties of existing phases and their global interactions. For this purpose, around 180 nanoindentation tests were performed on the coating surface to cover enough grains. The principle target in these experiments was to capture all the existing phases using nanoindentation with a relatively high collected statistical data.

Example of force *versus* displacement into surface curves associated with nanoindentation tests conducted on various phases are shown and compared in Fig. 2. Based on these curves one can notice that, the micromechanical behavior and work hardening of each phase is essentially different from each other. Zinc phase exhibits the highest penetration depth and lowest slope of loading profile among the phases by applying the same magnitude of normal force. Higher penetration depth of the indenter can be observed for the ternary eutectic compared to the binary eutectic. This pronounced difference perceived by nanoindenation experiments establishes the main basis to link the microstructure and mechanical behavior of the coating. To elaborate, the mean results of about 180 nanoindentation experiments are summarized in Fig. 3.

As shown in Fig. 3a, the sequence of elastic modulus magnitudes are revealed as follows: $E_{Zn} > E_{TE} > E_{BE}$. It is important to note that, the error bar associated with the elastic modulus of primary zinc grains is larger than those of the other existing phases. This scattering is mainly attributed to the crystal anisotropy of hexagonal close packed (HCP) zinc grains. The binary eutectic particularly consisting of high fraction of $MgZn_2$ phase exhibits the lowest elastic modulus among the constituents. However, as depicted in Fig. 3b, an inverse trend is found for the hardness values *i.e.* $H_{BE} > H_{TE} > H_{Zn}$. This is mostly attributed to the presence of hard $MgZn_2$ phase (with low elasticity) within the eutectics. In order to achieve a plastic deformation-based insight, it is essential to have access to yielding and straining information of the microstructure components in addition to elastic properties. Here, strain hardening exponent (n) is chosen as the main indication of microscale ductility extent. As presented in Fig. 3c, zinc grains deliver the highest average n-value (0.34) among all the phases ($n_{Zn} > n_{TE} > n_{BE}$). Very low magnitude of n (0.08) associated with the binary eutectic demonstrates the low tendency of this phase to withstand plastic deformation. On the other hand, considering results given in Fig. 3d, the binary eutectic exhibits the highest yielding stress among the constituents ($\sigma_{BE} > \sigma_{TE} > \sigma_{Zn}$) identical to the obtained hardness trend. Therefore, in spite of having high yield strength, the binary eutectic is appeared as the most detrimental constituent in terms of micro-ductility response. This behavior is mostly governed by the presence of hard but brittle $MgZn_2$ phase
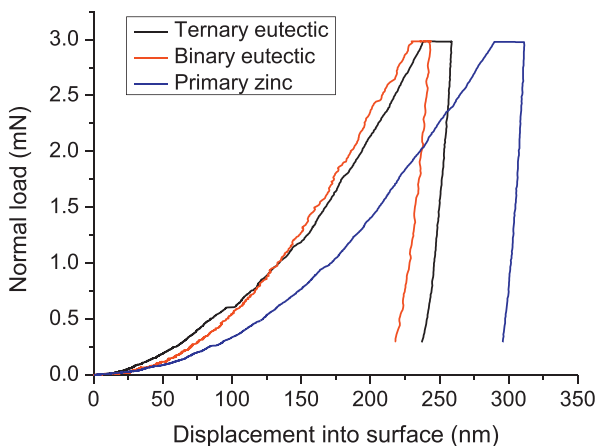
which is known as a non-deformable intermetallic in room temperature. It is significant to mention the fact that there exist scatters in the obtained nanoindentation results; however, from a comparative point of view, the discussed correlations are valid owing to the large number of statistical data of nanoindentation on the microstructural phases and the pronounced micromechanical differences observed in the loading profiles. The observed scatter may arise from the fact that, some indents might be situated on phase/grain boundaries of present phases [28]. In addition, the crystal anisotropy of both hexagonal Zn and $MgZn_2$ grains may have influenced the achieved results (this topic will be studied extensively in the following sections).

In order to take the influence of crystallographic orientation on local mechanical properties into account, OIM analysis was conducted on the nanoindented regions and one example is given in Fig. 4. As it can be observed in Fig. 4a and b, several zinc grains of different crystallographic orientations are covered by nanoindentations. Another significant observation is that the eutectic zinc phases normally follow the same orientation of the adjacent parent zinc grains. It is important to note that each dendrite of zinc phase may contain some sub-grains. This might be attributed to recrystallization of fine zinc grains during production of the coating in continuous hot-dip galvanization. As depicted in Fig. 4c, kernel average misorientation (KAM) intensity is found to be higher in the indented regions (revealing red color) indicating severe lattice distortion induced by nanoindentation. Moreover, regions with high density of grain boundaries display higher KAM values. Another remark is the presence of some tensile twins typically following direction of $[\bar{1}\,2\,\bar{1}\,0]$ in the microstructure, which most probably are formed during hot-dip galvanization as shown in Fig. 4d.

To link the micromechanical properties of individual grains obtained by nanoindentation with crystal orientation determined with OIM, the orientation angle, θ, is defined as the angle between the hexagonal c-axis of Zn grains and the loading (indentation, tension) direction. Accordingly, the corresponding local strain hardening exponents (n-values) of Zn grains attained by nanoindentation *versus* the measured θ values are plotted in Fig. 5. It is worth mentioning that, for each data point given in Fig. 5, depending on the availability of the indented grain orientations, at least four indented grains with close HCP crystal orientation to [0001] direction were considered and the average amount of corresponding n-values was used.

As it can be noticed, measured n-values exhibit an increasing trend with respect to θ. Accordingly, a forth order polynomial was fitted on the data points ($R^2 = 0.98$) and the expression was found as follows:

$$n = 1.428 \times 10^{-8}\theta^4 - 2.233 \times 10^{-6}\theta^3 + 1.027 \times 10^{-4}\theta^2 - 4.631 \times 10^{-4}\theta + 0.29 \tag{1}$$

where θ is the orientation angle of Zn grains, *i.e.* the angle between the hexagonal c-axis of Zn grains and the applied loading (indentation, tension) direction, and *n* is the strain hardening exponent. Therefore, as a consequence of HCP mechanical anisotropy, a plastic deformation parameter (n-value) was successfully linked to crystal orientation. This empirical equation enables revealing the deformation behavior at microstructural scale and therefore to evaluate micro-ductility response of zinc grains undergone specific deformation test. This equation can also be applied to evaluate the micro-ductility of other zinc-based alloys. The trend observed in Fig. 5 seems to be consistent with the reported elastic modulus variations with respect to the anisotropy of Zn crystals [29].

3.2. Crack initiation behavior

3.2.1. In-situ tensile and bending tests

Chronological observation of the coating microstructure subjected to tension is a key factor to scrutinize the origin of cracking in ZnAlMg coatings. To achieve this, *in-situ* SEM uniaxial tensile experiment is
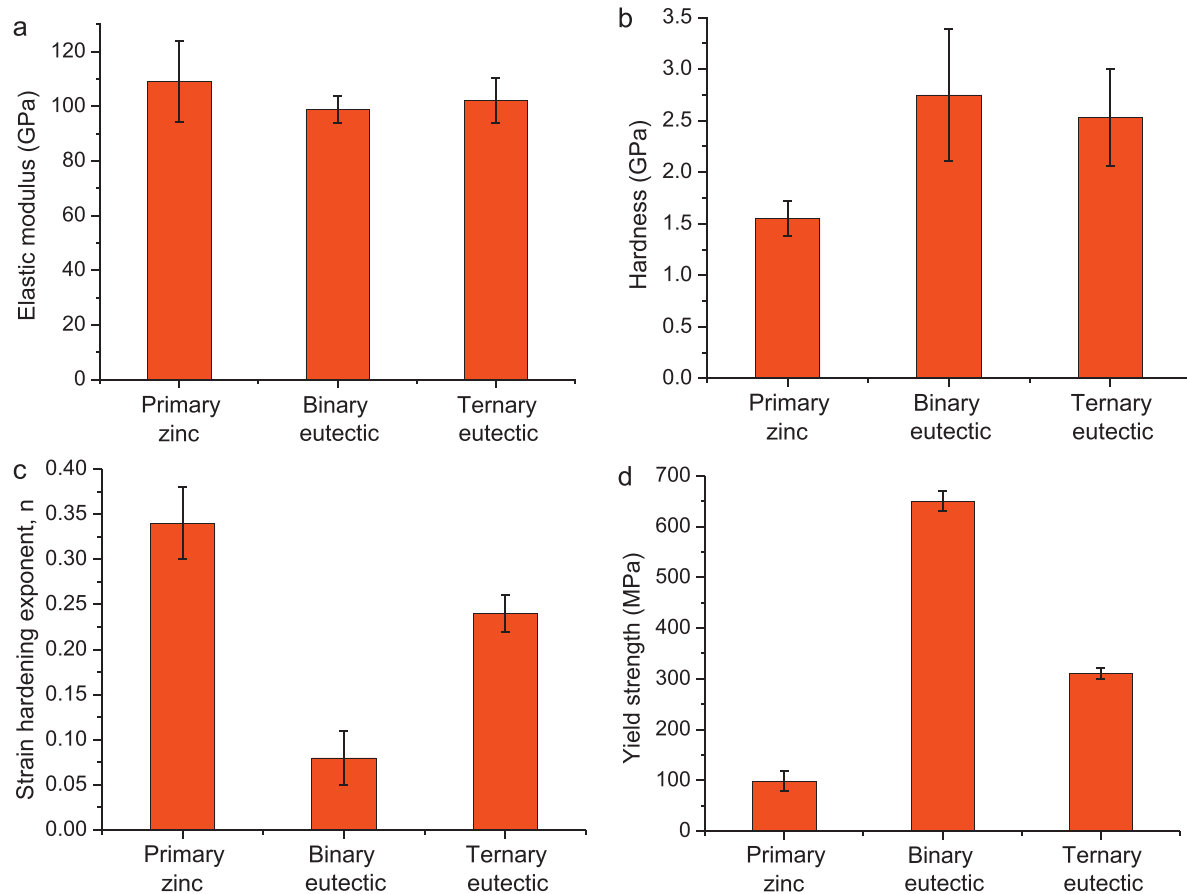

Fig. 2. Typical force *versus* displacement into surface profile for different phases of ZnAlMg coating obtained by nanoindentation test.

Fig. 3. Local mechanical properties obtained by nanoindentaion associated with different phases of ZnAlMg coating: (a) elastic modulus; (b) hardness; (c) strain hardening exponent and (d) yield strength.

conducted in such a way that cracking evolution can be traced locally. A ROI at the gauge length center of ZnAlMg coated steel tensile specimen was selected and tracked while performing the tensile tests at multiple intervals. The true stress-strain curve of Zn1.8Al1.8Mg coated steel obtained by tensile test is given in Fig. 6a. As revealed, the steel substrate exhibit Lüders band behavior (Upper yield strength = 410 MPa) in the early stages of the plastic deformation followed by strain hardening up to $\varepsilon = 0.21$, reaching the ultimate tensile strength 508 MPa. The SEM micrographs of ROI evolution at selected critical intervals during *in-situ* tension are illustrated in Fig. 6b–d (the tensile direction is horizontal). As it can be observed in Fig. 6c, by applying 1.5% strain on the substrate/coating system, first micro-cracks start to nucleate at the binary eutectic (shown by circles in Fig. 6c) throughout the ROI of the coating microstructure. The cracking initiation corresponds to the global stress of 400 MPa occurring in the Lüders region described in Fig. 6a. The pronounced crack initiation can be explained by the nanoindentation results discussed in Section 3.1. As it has been demonstrated, despite exhibiting high yield stress value, the binary eutectic offers the lowest micro-ductility among all the phases due to the presence of brittle $MgZn_2$ intermetallic. It is significant to note that, the attained flow curve of the substrate/coating system is mostly controlled by the much thicker steel substrate. Therefore, the measured global stress/strain may differ from the actual stress/strain magnitudes imposed within the thin ZnAlMg coating microstructure. In addition, deformation of the steel substrate having Lüders behavior can generate an inhomogeneous stress field over the coating leading to stress/strain localization. The possible negative effect of Lüders banding behavior of the steel substrate on the cracking of ZnAlMg coating has been shown previously [30]. In particular, the binary eutectic comprising of a ductile component (Zn) and a brittle component ($MgZn_2$) experiences latent stress contrast in its constituents resulting in early failure. In other words, very thin lamellas of binary eutectic prescribe a size effect in which dislocation source for slip is limited leading to early fracture of this phase. These explanations can contribute to illuminate the early fracture of binary eutectic at around 400 MPa global stress, in spite of exhibiting high yield stress (650 MPa) estimated by nanoindentation method. As deformation proceeds to 15% global strain, the formed cracks are mostly widened and arrested by the adjacent Zn grains. Most of the primary zinc grains seem to be able to accommodate the applied deformation, yet there exist some damages in a few zinc grains indicated by red circles in Fig. 6d. In order to figure out the contributing factors determining the cracking tendency of primary Zn grains, detailed EBSD analysis is conducted and will be discussed further in Section 3.4.

In addition to *in-situ* tensile experiments, some *in-situ* bending (buckling) tests are also performed to evaluate the bendability of the ZnAlMg coatings. Fig. 7a depicts the microstructure of the coating after 15° bending. As it can be observed, all of the cracks initiated in the binary eutectic in transgranular mode confirming the previous observations regarding less-ductile binary eutectic phase in tensile test. The pronounced discrepancy of mechanical properties between the binary eutectic and primary zinc grains resulted in arresting the microcracks at the binary eutectic/primary Zn interface at small bending angle up to 15°. By increasing the bending angle to 30°, some more cracking incidents take place within the microstructure as presented in Fig. 7b. The initiated crack in the binary eutectic further propagates through primary Zn and may be deflected towards another Zn grain on its path. In spite of not detecting any crack deflection in tensile tests, here the cracking behavior seems to be different in bending mode exhibiting both propagation and deflection. However, as it can
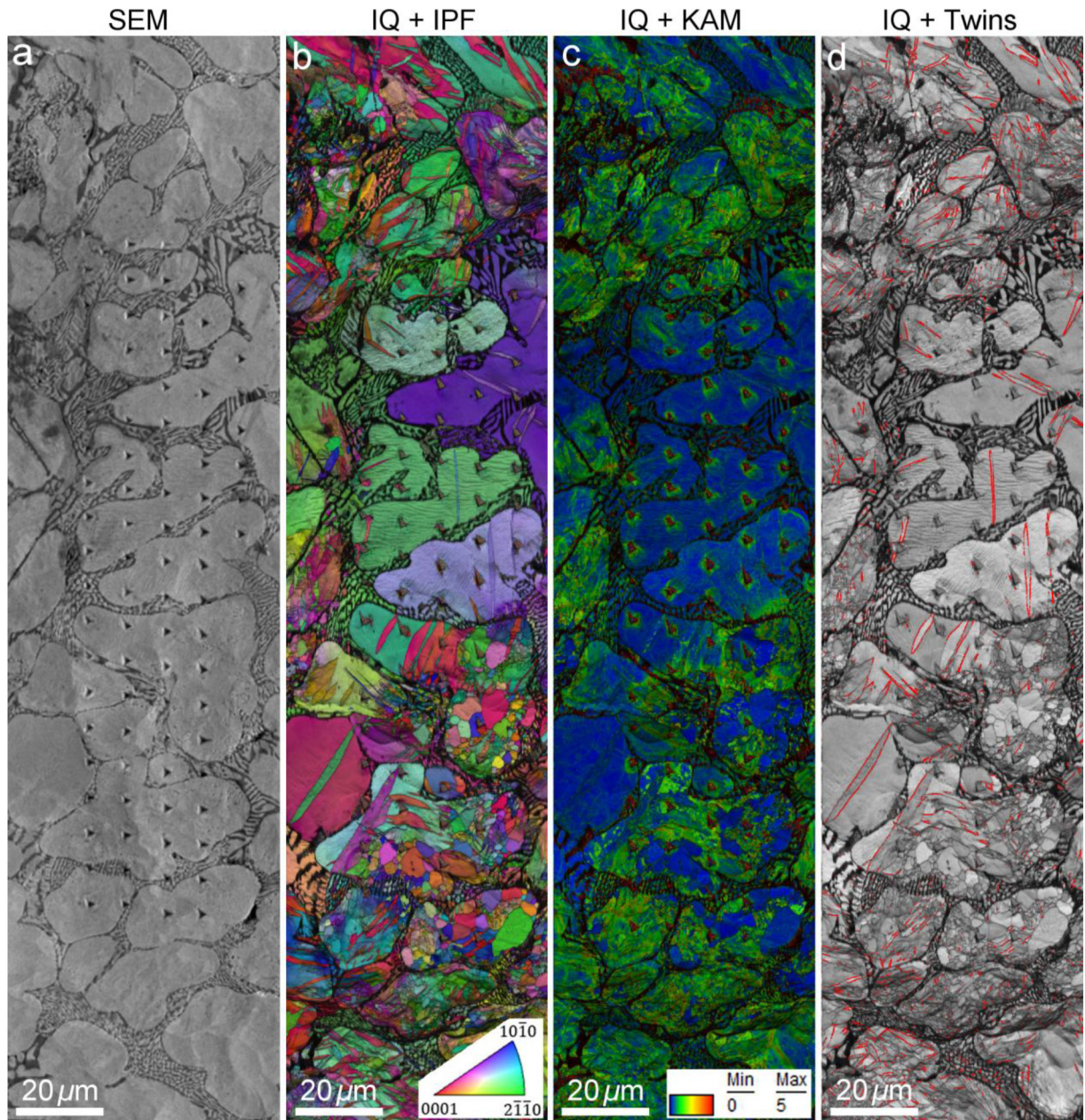
Fig. 4. OIM analysis on a nanoindented region: (a) SEM micrograph, (b) image quality plus inverse pole figure map, (c) image quality plus kernel average misorientation map and (d) image quality plus twinning map (twin boundaries are indicated by red lines). (For interpretation of the references to color in this figure legend, the reader is referred to the web version of this article.)

be noticed in Fig. 7b, not all the Zn grains may serve as propagation or deflection cracking sites for the initiated micro-crack.

3.2.2. DIC analysis

The obtained global strain by means of *in-situ* tensile test incorporates the mechanical response of both the steel substrate and ZnAlMg coating. Certainly, the measured global strain may differ from the actual strain values and distributions within the coating microstructure undergone tension. Digital image correlation (DIC) can assist in evaluating the micro-mechanical behavior of individual microstructure constituents [31]. Fig. 8a illustrates the decorated ROI of the coating microstructure prior to *in-situ* tensile/μ-DIC analysis. The ROI is composed of fair amount of primary Zn, binary eutectic and ternary eutectic with the typical distributions within the coating microstructure. Fig. 8b demonstrates the overlaid DIC strain map on the ROI after applying 1% global tensile strain.

Some interesting phenomena can be detected using this analysis. The imposed tensile deformation on the coating led to heterogeneous strain partitioning within the coating microstructure. Most of the strain accumulation takes place over the binary and ternary eutectics rather than the primary zinc grains. Although both binary and ternary eutectics experienced severe strain localization, in the case of binary eutectics it mostly leads to crack initiation with large opening due to its low micro-ductility. In spite of exhibiting highly deformed zone, ternary eutectic seems to accommodate the applied deformation without exhibiting crack at this stage. On the other hand, a nucleated crack within the binary eutectic is detected as designated in Fig. 8b. Nevertheless, some primary zinc grains may also tolerate strain localization due to their non-favorable crystallographic orientations for plastic deformation. This issue will be discussed in details by using EBSD analysis on the cracked zinc grains. It should be noticed that, narrower strain concentration is developed regarding primary Zn grains compared to the
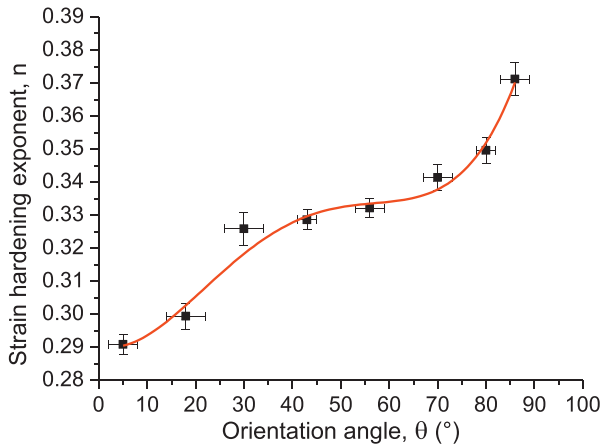
Fig. 5. Variation of local strain hardening exponent with zinc crystal orientation.

which micro-cracks were initiated was also captured using DIC analysis, typically in the range of 0.03–0.04.

3.2.3. Finite element analysis (FEA)

In order to estimate the local stress distribution and predict the cracking initiation within the microstructure of ZnAlMg coating, a set of extended finite element method (XFEM) simulation was performed on a two dimensional (2D) microstructure representation. The generated 2D FEM model, experimental ROI subjected to tension, von Mises stress field result and shear stress distribution are illustrated in Fig. 9.

The XFEM results imply that, most of stress concentration is substantially generated in the binary eutectic as shown in Fig. 9c. A severe stress localization can be noticed in the brittle binary eutectic between the two adjacent Zn grains reaching a maximum 692 MPa. By meeting the critical point required for crack initiation (around 1% tensile strain), the binary eutectic begins to crack perpendicular to the loading direction. This simulation agrees well with the experimental observation of the ROI given in Fig. 9b. As indicated by arrows in Fig. 9d, due to the large variation of mechanical properties between the primary zinc and binary eutectic, severe shear stress concentrations are created at the phase boundaries. Therefore, large difference of mechanical properties (i.e. yield strength and micro ductility) in the coating microstructure seems to be detrimental for the formability of the coating and facilitate the cracking phenomenon during tension. A more homogenized microstructure incorporating phases with high micro-ductility (i.e. primary zinc and ternary eutectic) seems to be helpful to restrain the stress localization and subsequently to delay/hinder cracking initiation in ZnAlMg coating. It is worth mentioning that, integrating the extended
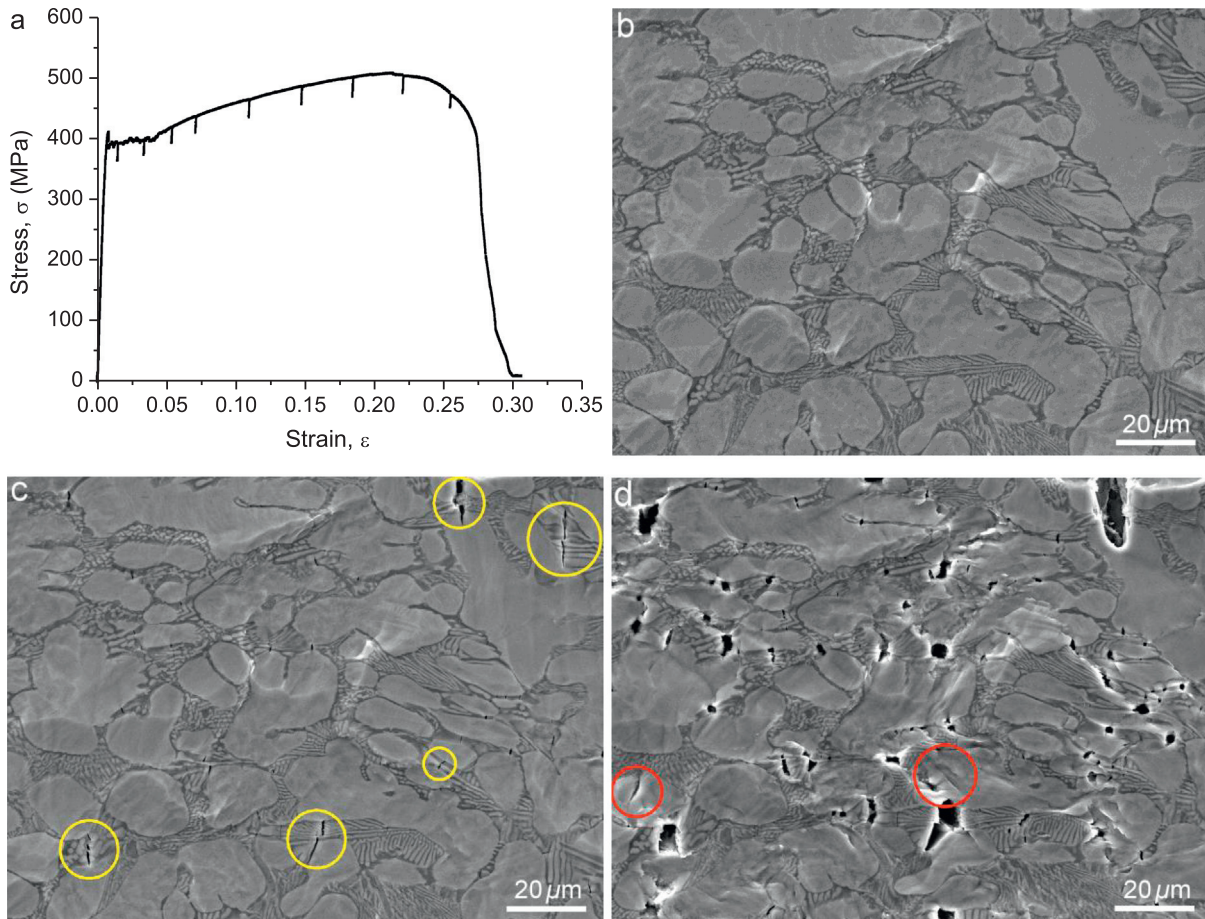
eutectics. The pronounced strain distribution contrast could be also influenced by deformation-driven effects from underlying steel substrate. Since the conducted DIC analysis lies in the early stage of Lüders band region of the steel substrate (onset of crack initiation in the coating), heterogeneous stress/strain transfer from substrate to the coating may play a significant role in the observed strain field in the ROI. In other words, the coating microstructural components fail to accommodate the multiaxial stress generated by the underling substrate [32]. In addition to obtaining strain field mapping, the precise local strain value at

Fig. 6. (a) True flow curve obtained for ZnAlMg coated steel using in-situ SEM uniaxial tensile test; (b) SEM image of the ROI prior to in-situ uniaxial tensile test; (c) the ROI after 1.5% strain and (d) the ROI after 15% strain (The tensile direction is horizontal).
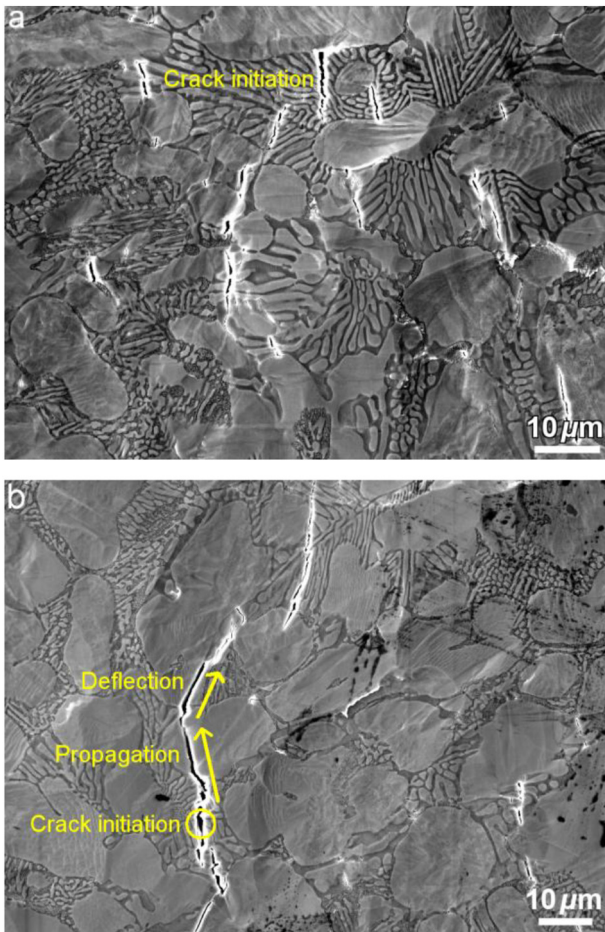
Fig. 7. SEM observation in bending ZnAlMg coating sample: (a) bent to 15° encompassing crack initiation in the binary eutectic; (b) bent to 30° revealing crack propagation and deflection.

finite element model with crystal plasticity approach can further improve the prediction of cracking behavior of ZnAlMg coatings, which is not the main focus in this work.

3.3. Damage development and deformation analysis

Damage development and deformation mechanisms as the integrated result of micro-mechanical properties and crystallographic orientation are studied intensively using *in-situ* EBSD analysis next. As the consequence of high mechanical anisotropy, low symmetry and hexagonal unit cell, zinc-based alloys normally exhibit heterogeneous deformation as the five independent slip systems required for von Mises criterion fail to be satisfied [23]. The reported [33] principal slip systems of HCP zinc are depicted in Fig. 10. Second order pyramidal and twining may also add to these deformation mechanism based on the condition of the loadings [17].

To scrutinize the microstructural evolution, deformation mechanism and damage development in ZnAlMg coating, a set of uniaxial tension combined with real time *in-situ* EBSD analysis was exploited. Fig. 11 demonstrates the results of *in-situ* EBSD analysis on a chosen ROI in the center of the gauge length of tensile specimen. The experiment was conducted in three stages, *i.e.* ROI prior to deformation (Fig. 11a), ROI at 0.5% tensile strain (Fig. 11b) and at 2% tensile strain (Fig. 11c). Each part of Fig. 11 encompasses the following items: corresponding SEM micrograph, image quality (IQ) plus inverse pole figure (IPF) map, IQ plus Schmid map, IQ plus local orientation spread (LOS) map and finally LOS distribution chart of each test stage which are also written on the top of Fig. 11.
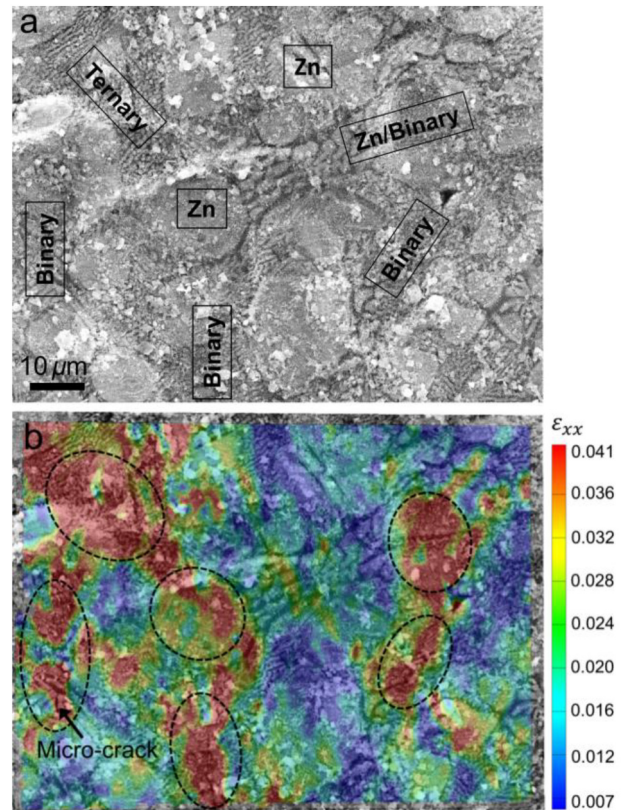

Fig. 8. (a) SEM micrograph of YSZ nanoparticles decorated ROI before performing *in-situ* tension/μ-DIC test; (b) DIC strain map of the ROI at 1% global tensile strain (the tensile direction is horizontal).

As Fig. 11a depicts, the chosen ROI prior to deformation consists of three typical constituents *i.e.* primary Zn, binary eutectic and ternary eutectic indicated by arrows in the SEM micrograph. Some twins are also visible in the primary zinc parent grains as indicated in the IPF map. Concerning Schmid maps in Fig. 11, it is important to state that, the principle Zn slip systems displayed in Fig. 10 (including all the equivalent crystallographic families) were considered and the corresponding Schmid maps were calculated and plotted according to tensile principle stress state along rolling direction (RD). As shown in Schmid map of Fig. 11a, Zn grains numbered 1 and 2, exhibit a high Schmid factor (m) 0.48, whereas their twining products have a low m-factor 0.21. In contrast, Zn grain No. 3 exhibits low m-factor equals to 0.19. LOS distribution chart and map of ROI prior to deformation suggest that, the number fraction of low orientation spread (0–1°) is predominantly high. By applying 0.5% tensile strain, the number fraction of intermediate orientation spread (1–2°) becomes dominant as described in Fig. 11b. As the deformation proceeds to 2% tensile strain, more microstructural evolution is occurred as presented in Fig. 11c. The needle-like twins are coalesced and grown within their parent grains as the consequence of lack of available slip deformation. In principle, the ratio of critical resolved shear stress (CRSS) among basal slip and twining is described as 1:15 [17]. Thus, the principle slip systems presented in Fig. 10 seemly fail to prevail as dominant deformation mechanisms in some regions and subsequently an alternative deformation twinning is activated. The number fraction of high angle LOS (2–3°) is substantially increased in this stage compared to the previous steps. The most concentrated sites of high LOS values are designated by arrows in the LOS map in Fig. 11c. Grain No. 3 with a low m-factor, twin boundaries and binary eutectic experienced high LOS concentration. Moreover, reaching the required strain/stress for crack initiation in this step, some micro-cracks are formed in the binary eutectic as shown in the SEM micrograph (Fig. 11c). The origin of these micro-cracks are revealed in MgZn₂ platelets in the magnified
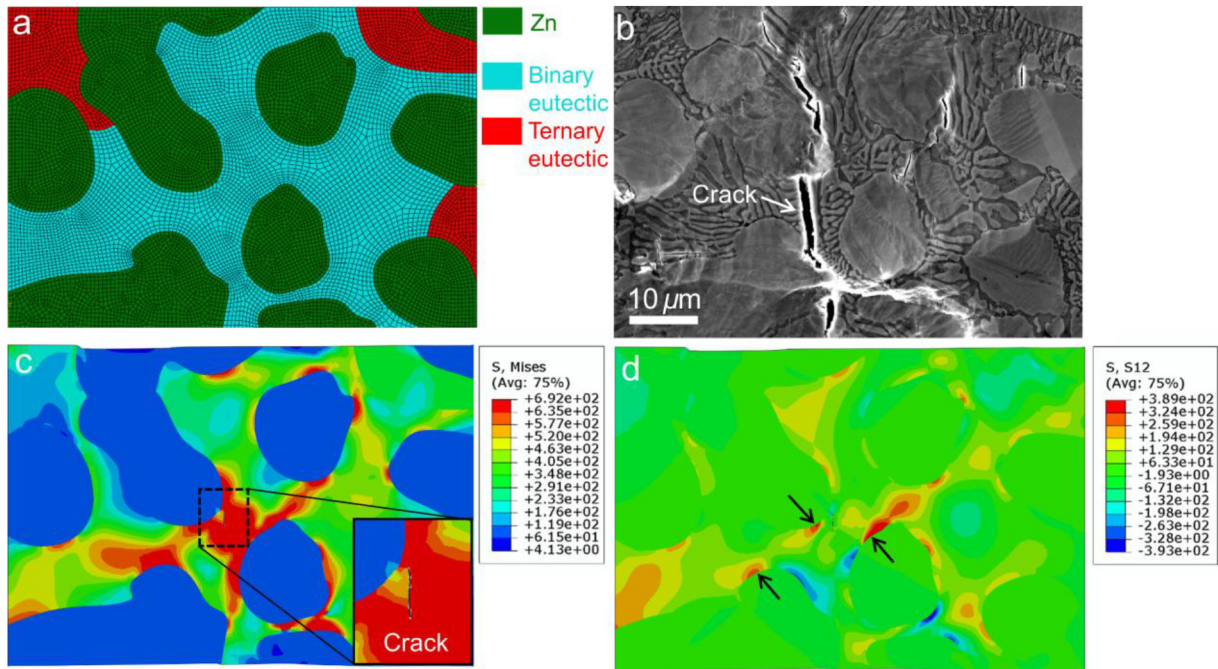
Fig. 9. Finite element analysis simulation results: (a) meshed model incorporating microstructural constituents of ZnAlMg coating, (b) SEM micrograph of the ROI at 1% tensile strain, (c) von Mises stress distribution and (d) shear stress field (the tensile direction is horizontal).

SEM image. Interestingly, the cracked sites in the ROI exhibit high LOS values in their vicinity as indicated by dashed ellipses in LOS map. Therefore it is noticed that, the higher the LOS value, the higher the probability of the microstructural features to suffer damage and cracking. Twin boundaries and Zn grains with low m-factor are revealed as two other potential sites for damage development within ZnAlMg coating microstructure. It should be noticed that, despite measuring relatively high m-factor (0.42) associated with the binary eutectic, it has undergone cracking during the imposed plastic deformation. This is probably attributed to the fact that, the binary eutectic is comprised of brittle and non-deformable $MgZn_2$ platelets which are not considered in the calculation of Schmid factor. Therefore, the Schmid factor criterion is only applicable for the deformation analysis of the primary Zn grains in this study. To scrutinize the cracking genesis in the binary eutectic, regardless of crystallographic orientation parameter, it is necessary to take into account the residual tensile stress built within the thin platelets as the consequence of difference in the coefficient of thermal expansion (CTE) during solidification of Zn and $MgZn_2$ constituents

[24], or pronounced solidification shrinkage [34] resulting in microcrack formation in the thin lamellas. Some evidences of such hypothesis are provided in the supplementary data (see Fig. S4).

3.4. Cracking mechanism

In addition to the cracking genesis in ZnAlMg coating system studied in this work, the cracking mechanism of the primary Zn grains is essential to investigate. As it is manifested in Section 3.2.1, some primary Zn grains may experience damage during deformation and result in large open cracks. To elaborate on the cause for this phenomenon, EBSD analysis is conducted on the regions encompassing cracked Zn grains. Fig. 12 depicts the EBSD results of a cracked area after 10% strain subjected to uniaxial tension, and Figs. 13–15 demonstrate EBSD results of three different cracked areas on a coating sample bent to 30°. All these figures include image quality (IQ), IQ plus inverse pole figure (IPF), the corresponding Schmid map and HCP unit cells of the critical numbered grains. For the bent sample, the same procedure is followed for Schmid factor calculation as described earlier, assuming dominant tensile stress regime on the top free surface of a bent specimen [35,36]. The detailed crystallographic orientation and micro-mechanical information of all labeled grains with numbers are given in Table 1. Using the expression (Eq. 1) established on orientation-micromechanical properties relationship in Section 3.1, strain hardening exponent of various grains is calculated and reported in Table 1. It should be noted that, the n-values are calculated by measuring θ - HCP orientation angle with respect to RD (parallel to the tensile direction) - and plugging in Eq. (1).

According to the results given in Fig. 12 and Table 1, all the Zn grains with a low m-factor and low n-value experienced transgranular cracking during tensile test. For instance, grain No. 1 having c-axis almost parallel to the tensile direction or RD (θ = 2.1°), exhibited a very low strain hardening exponent ($n = 0.289$) and also quite low Schmid factor (m = 0.03), oriented unfavorably and consequently experienced cracking. On the other hand, grain No. 3 possessing a high n-value 0.368 and a pretty high m-factor accounts to 0.44 exposed as a favorable orientation to accommodate plastic deformation without enduring cracking. In addition, the formed cracks in grains No. 1 and 2 are arrested at the boundaries of adjacent grains with a high m-factor. Fig. 13 (area No. 1) delivers
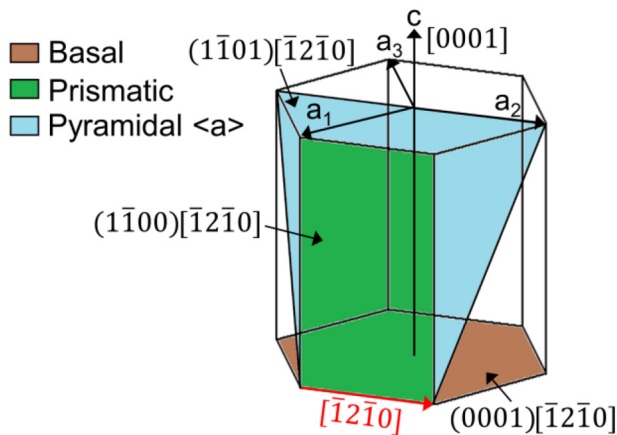

Fig. 10. Principal slip systems of HCP Zn crystal implemented for the calculation of Schmid factor (m).
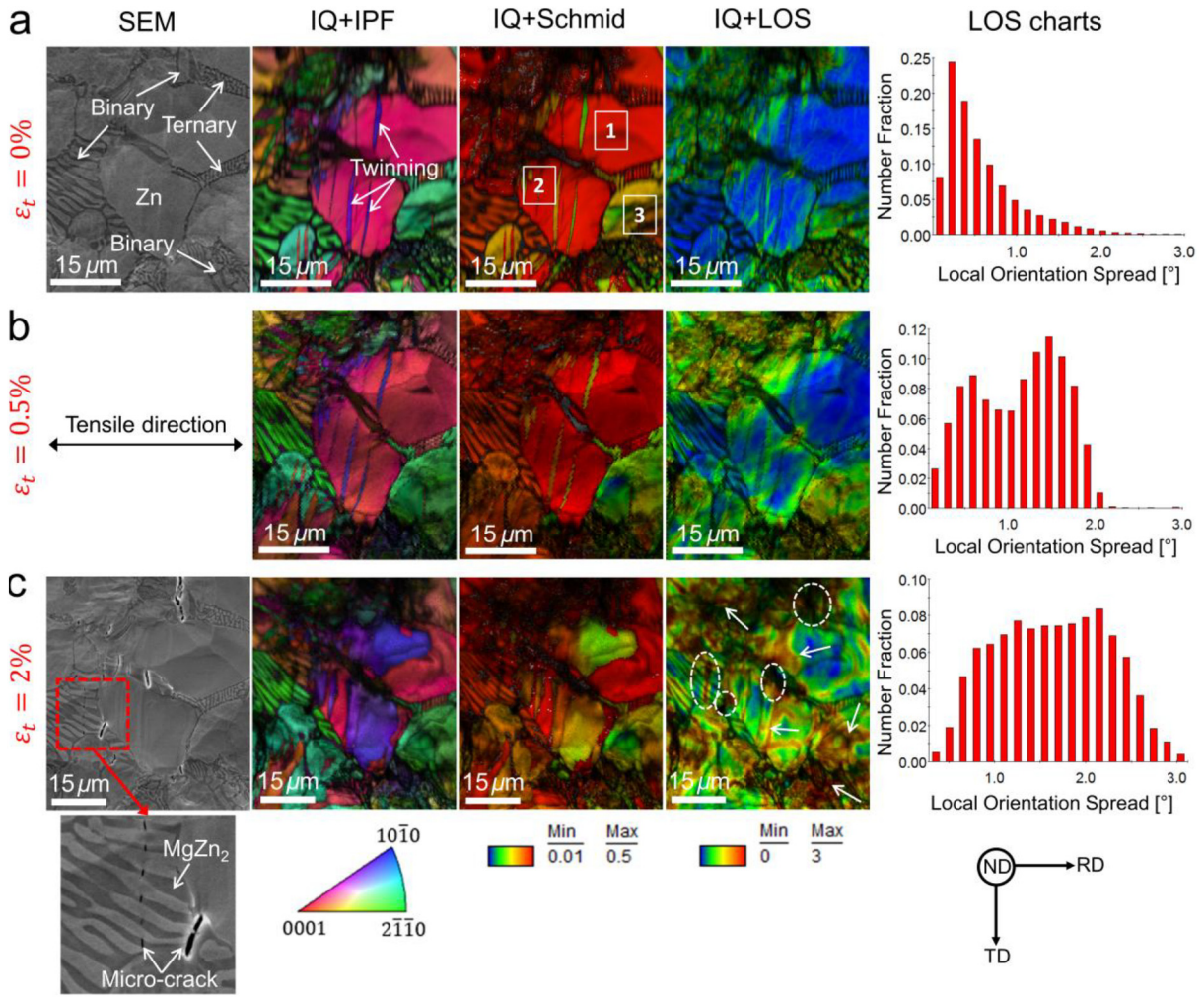
Fig. 11. *In-situ* tension and OIM analysis: (a) a ROI prior to deformation, (b) the ROI at 0.5% global tensile strain and (c) the ROI at 2% global tensile strain.

more insight towards the cracking of the microstructure subjected to bending. The observed crack in this figure, seems to be initiated in MgZn₂ phase and further propagated through the neighbor Zn grains.

Grain No. 1 oriented with c-axis nearly parallel to RD exhibiting low m and n values, serves as an unfavorable orientation and underwent cracking. Whereas, the other adjacent Zn grain (No. 2), possessed an
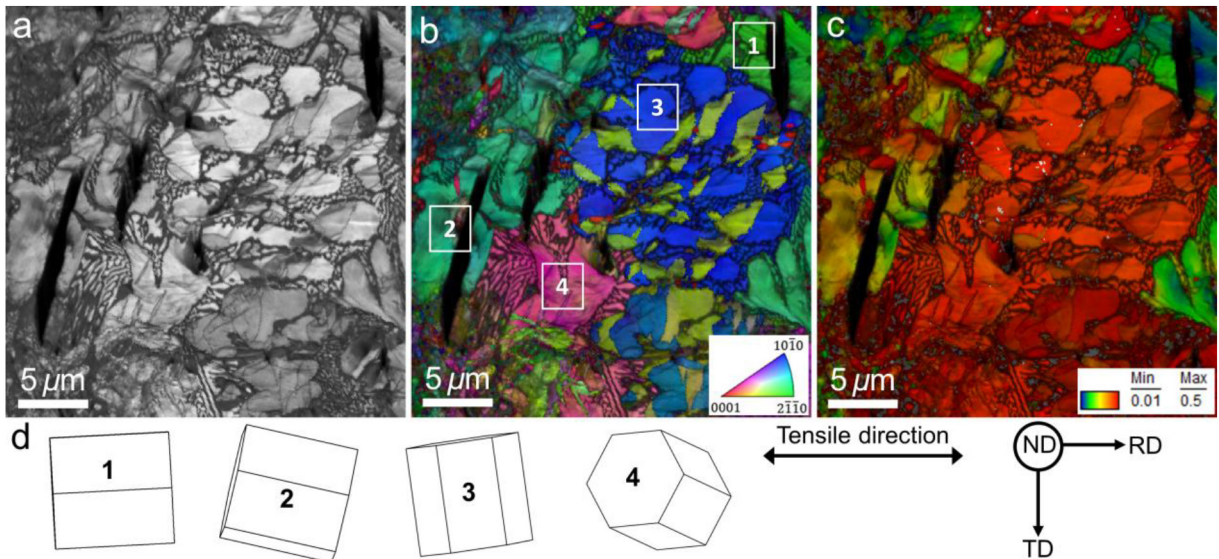

Fig. 12. OIM analysis on a cracked area after uniaxial tension: (a) image quality (IQ); (b) inverse pole figure (IPF) map over IQ, (c) Schmid map plus IQ and (d) selected HCP crystals of numbered Zn grains.
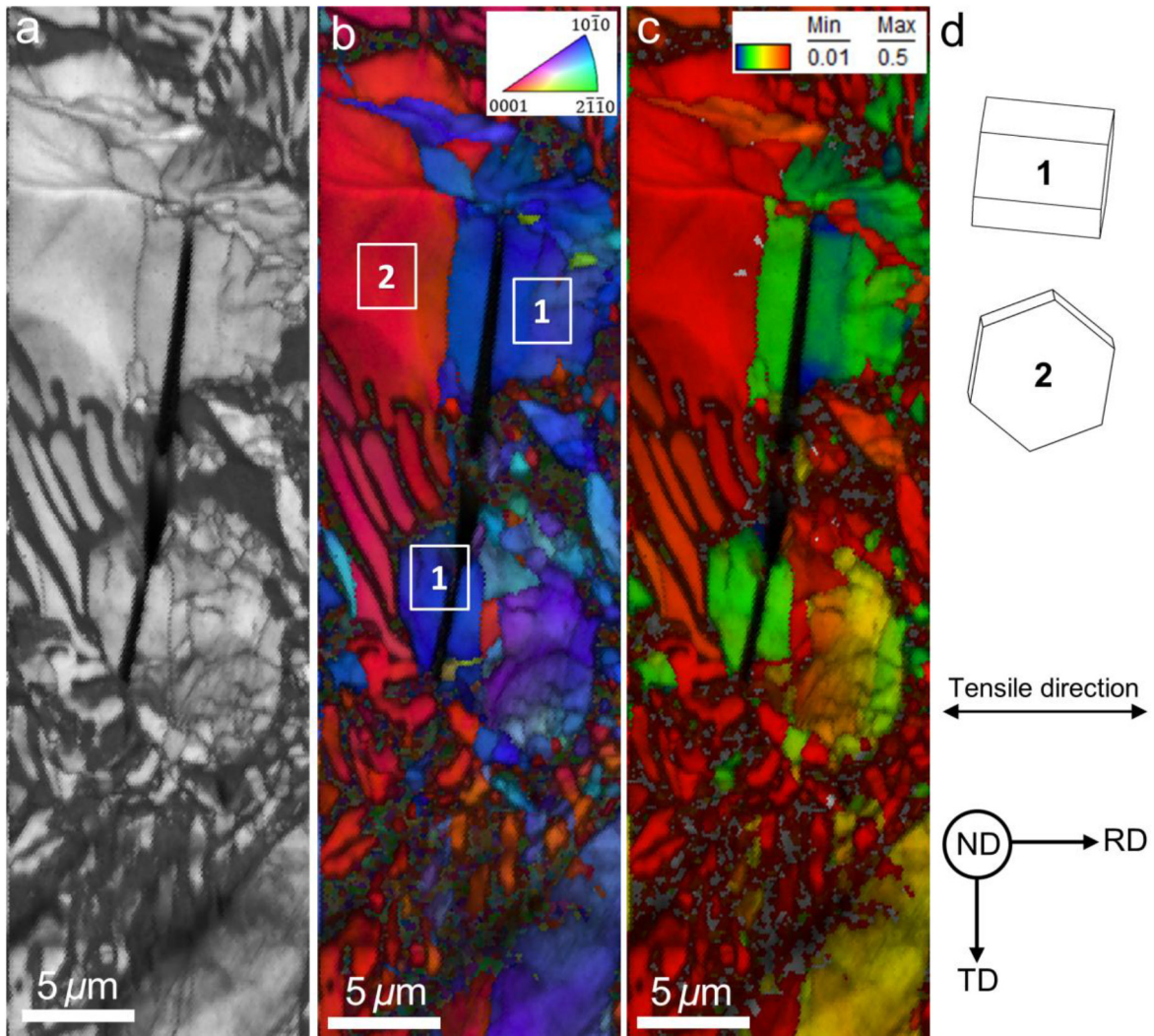
Fig. 13. OIM analysis on the cracked area No. 1 after bending: (a) image quality (IQ); (b) inverse pole figure (IPF) map over IQ; (c) Schmid map plus IQ and (d) selected HCP crystals of numbered Zn grains.

orientation with c-axis perpendicular to RD, and prevails as a favorable alignment for resisting crack propagation. Furthermore, Fig. 14 (area No. 2) confirms the previous observation indicating the importance of grain orientation to activate primary slip systems of HCP Zn and resulting in high m-factor to repel crack formation. The created crack in this area are also got arrested when reaching to a ductile Zn grain with high m-factor. Based on Fig. 15 (area No. 3), one can notice that, almost all the Zn grains with low m and n-values cracked perpendicular to RD after bending test. However, grain No. 5 with almost high m-factor (0.39) and intermediate strain hardening exponent ($n = 0.321$) displayed a cracking deflection site in the bent sample. This observation is mainly attributed to the fact that, the deformation gradient (including shear stress) in the bending test is more complicated than that of uniaxial tensile regime (the implemented stress state for Schmid factor calculations). The observed cracking deflection incidents are rarely seen in the coating microstructure and are only formed with a specific θ around 32° in bending mode rather than uniaxial tension. Hence in general, taking both m and n parameters into consideration, primary Zn grains with $m < 0.32$ and $n < 0.33$ display cracking during deformation. It is significant to notice that, by providing unfavorable orientation for global deformation, the observed cracks are all formed along the basal cleavage plane of Zn crystals. These (0001) cleavage planes are regarded as the most detrimental cleavage orientations for zinc-based alloys [37] leading to brittle fracture [38]. Based on the aforementioned results, the

spatial orientation of the primary Zn grains with respect to loading direction play an important role in extent of cracking in ZnAlMg coatings. An additional supportive EBSD results on a different cracked region is given in supplementary data (see Fig. S5).

4. Final remarks

In this paper we manifested that the micro-mechanical and crystallographic orientation dependent interplay between the microstructural constituents of ZnAlMg coating determines the origin and extent of damage and cracking within these coatings. To gain such end, we methodically introduced a plastic deformation-based approach to address the underlying mechanisms using specific criteria. These three plastic-deformation based criteria can be described as follows: (1) Different micro-ductility behaviors are revealed for various phases in the coating microstructure, indicating the binary eutectic as the most detrimental constituent in which most of the cracks initiate; (2) Primary Zn grains possess different magnitudes of local strain hardening exponents (n values) as a result of HCP zinc orientation angle (θ) correlated by Eq. (1). Accordingly, Zn grains with unfavorable orientations with respect to loading direction (exhibiting $n < 0.33$) endured cracking during tensile/bending deformations; (3) Based on the deformation mechanism analysis, Schmid factor field associated with coating microstructure was determined for tensile and bending modes. Correspondingly,
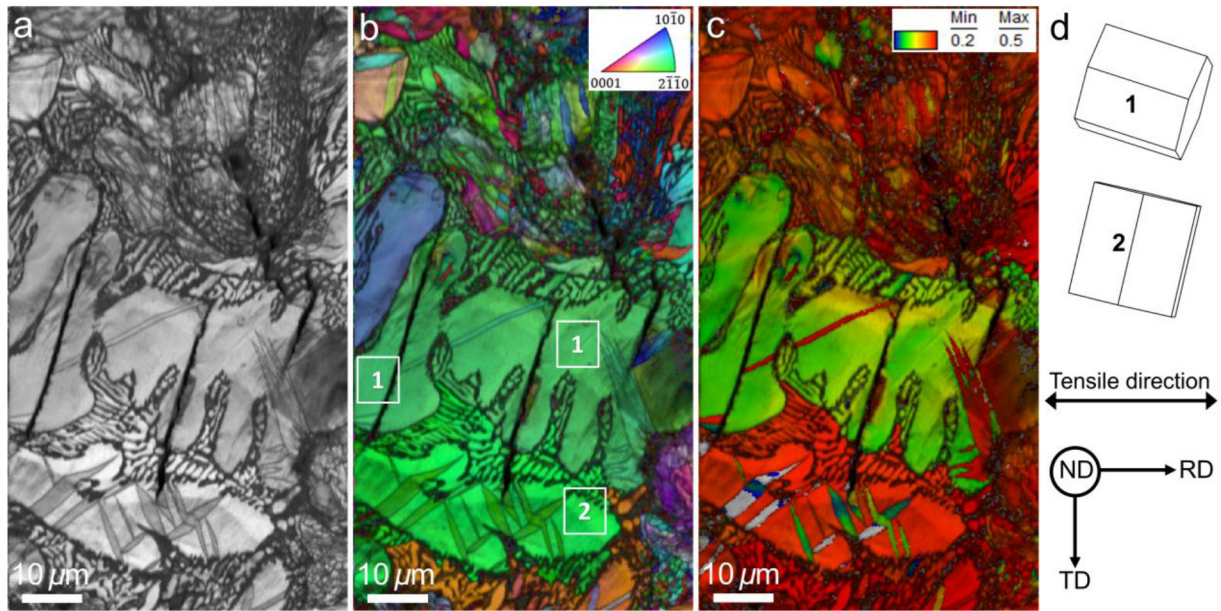
Fig. 14. OIM analysis on the cracked area No. 2 after bending: (a) image quality (IQ); (b) inverse pole figure (IPF) map over IQ; (c) Schmid map plus IQ and (d) selected HCP crystals of numbered Zn grains.

Zn grains with a low Schmid factor ($m < 0.32$) lacking dislocation motion for plastic deformation experience cracking. The collective package of the mentioned criteria offers a quantitative benchmark incorporating micromechanical properties, spatial orientation and deformation response to anticipate damage and cracking of ZnAlMg coating microstructure.
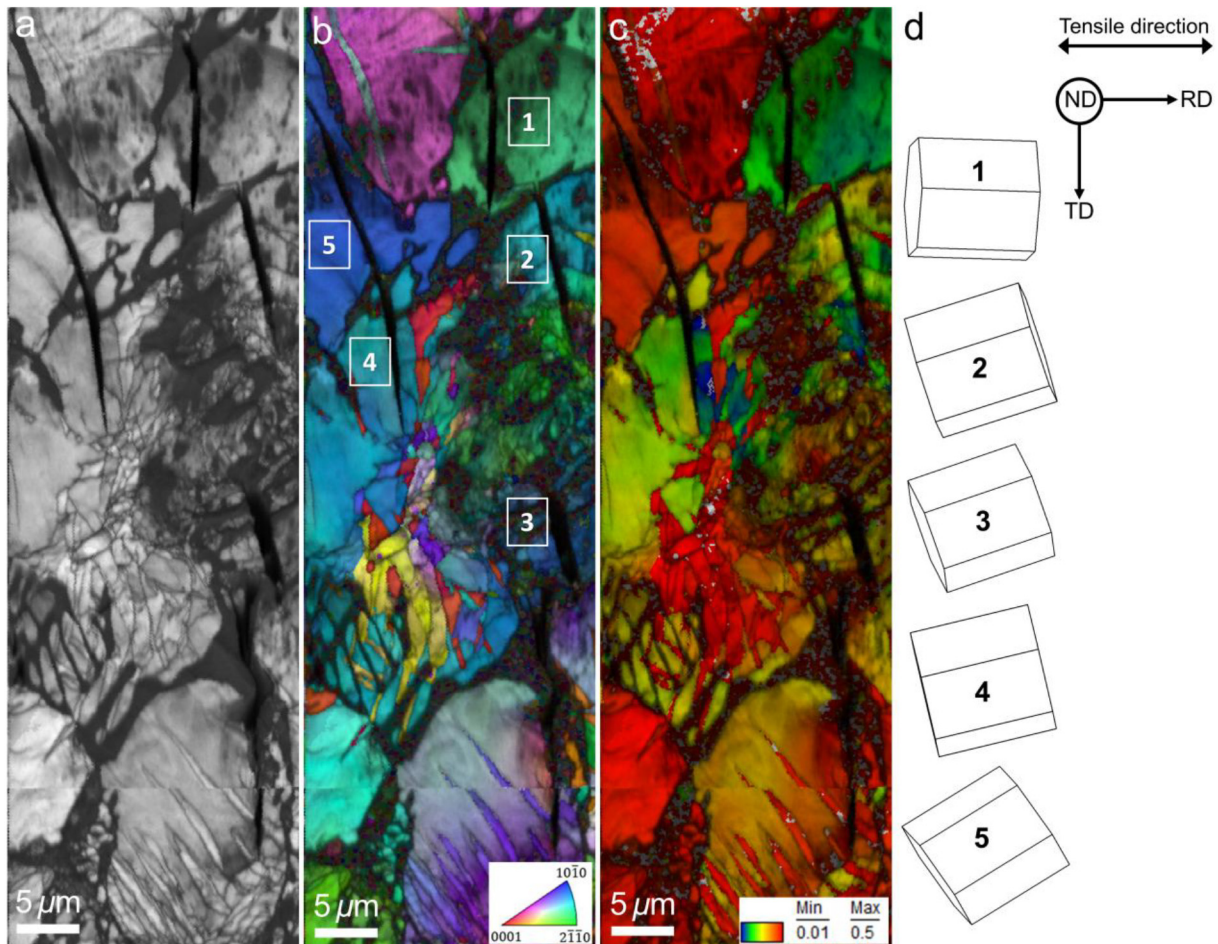

Fig. 15. OIM analysis on the cracked area No. 3 after bending: (a) image quality (IQ); (b) inverse pole figure (IPF) map over IQ; (c) Schmid map plus IQ and (d) selected HCP crystals of numbered Zn grains.

Table 1
Detailed crystallographic orientation and micro-mechanical information of all labeled grains.

Test	Area no.	Zn grain no.	Average grain orientation	Orientation angle, θ (°)	Schmid factor, m	Strain hardening exponent, n	Cracked?
Tensile	1	1	$(6\ \bar{1}2\ 6\ \bar{1})[1\ 0\ \bar{1}\ 0]$	2.1	0.03	0.289	Yes
	1	2	$(3\ 6\ \bar{9}\ \bar{1})[11\ \bar{9}\ \bar{2}\ \bar{3}]$	14.5	0.25	0.298	Yes
	1	3	$(\bar{3}7\ 1\ 36\ 2)[3\ \bar{5}\ 2\ 22]$	85.3	0.44	0.368	No
	1	4	$(\bar{5}\ 4\ 1\ 15)[\bar{8}\ \bar{4}1\ 49\ 5]$	63	0.42	0.335	No
Bending	1	1	$(\bar{3}5\ 32\ 3\ 3)[\bar{9}\ \bar{1}2\ 21\ 2]$	8.5	0.14	0.292	Yes
	1	2	$(0\ 1\ \bar{1}\ 23)[11\ 6\ \bar{1}7\ 1]$	86.4	0.49	0.371	No
	2	1	$(\bar{6}\ 9\ 15\ 5)[\bar{1}1\ 9\ 2\ \bar{3}]$	19.1	0.29	0.304	Yes
	2	2	$(10\ 12\ \bar{2}2\ \bar{1})[6\ \bar{5}\ \bar{1}\ 22]$	77	0.47	0.346	No
	3	1	$(\bar{4}\ 11\ \bar{7}\ 3)[\bar{6}\ 1\ 5\ 0]$	8.4	0.14	0.292	Yes
	3	2	$(\bar{4}\ 1\ 3\ 0)[\bar{4}\ 14\ \bar{1}0\ 3]$	15.3	0.26	0.299	Yes
	3	3	$(2\ 11\ \bar{1}3\ 2)[10\ \bar{6}\ \bar{4}\ 3]$	22.1	0.3	0.309	Yes
	3	4	$(\bar{5}\ 4\ 1\ 0)[\bar{3}\ 6\ 9\ \bar{2}]$	12.6	0.21	0.296	Yes
	3	5	$(\bar{1}2\ 13\ \bar{1}\ 2)[\bar{6}\ 4\ 10\ \bar{5}]$	32.5	0.39	0.321	Yes

To elaborate, a schematic representation of microstructural scale cracking behavior of ZnAlMg coatings is given in Fig. 16. Cracking path begins with nucleation of tiny micro-cracks in $MgZn_2$ platelets of binary eutectic as the result of strain localization in this region in stage I. As the deformation proceeds to a certain stress/strain threshold, these micro-cracks coalesce and grow mostly perpendicular to binary eutectic platelets (*e.g.* stage II in Fig. 16). When the crack reaches the interfaces between the primary Zn grains and binary eutectic, there might be two situations according to the *in-situ* evaluations performed earlier. The first circumstance is that the adjacent Zn grain (*e.g.* Zn grain No. 1 in Fig. 16) exhibits an orientation close to [0001] perpendicular to the loading direction, *i.e.* the cases given in Fig. 17a and b. In this situation, the primary slip systems of Zn grain are activated by easy dislocation motion and subsequently ductile plastic deformation takes place instead of cleavage cracking (assuming the force direction is parallel to RD). Consequently, the crack is arrested in the primary zinc grain boundary. On the contrary, the second circumstance is that the adjacent Zn grain possesses an orientation with HCP c-axis parallel to the loading direction (see Fig. 17c) and incorporates low m-factor and n values, serving as a favorable site for the propagating crack (*e.g.* cracked Zn

grain No. 2 at stage III, Fig. 16). In particular, by increasing of θ (the orientation angle of HCP c-axis with respect to the loading direction) from 0 to 90°, cleavage (brittle fracture) becomes less dominant, and principle ductile deformation mechanisms including basal dislocation slip effectively activate and prevent crack propagation. The mentioned cracking mechanism is associated with the coating undergone uniaxial tension. However, for bending mode, there might be an additional
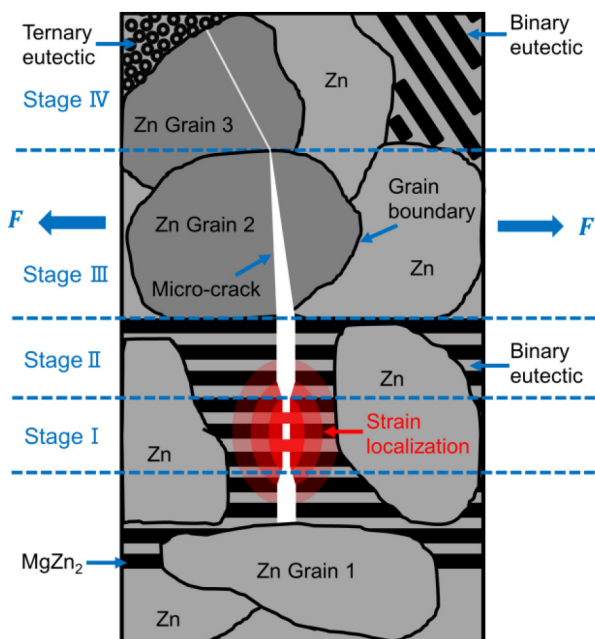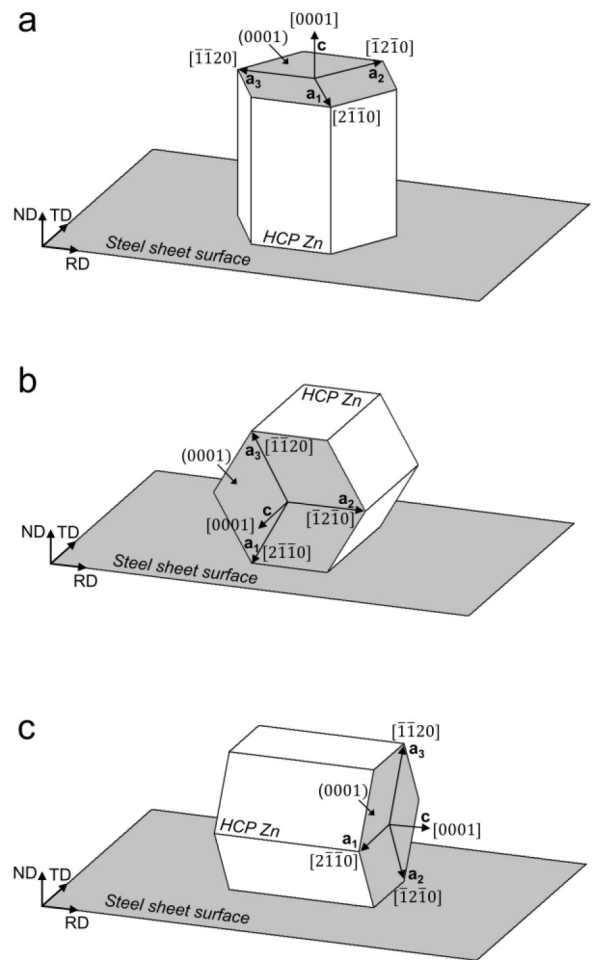

Fig. 17. (a) Zn HCP crystal orientation favored for cracking resistance type 1, (b) Zn HCP crystal orientation favored for cracking resistance type 2 and (c) Zn HCP crystal orientation leading to cracking (assuming the loading direction is parallel to RD).

Fig. 16. Schematic representation of the cracking mechanism in ZnAlMg coatings.

stage called crack deflection. Based on the attained results, if the neighbor Zn grain of a propagating crack is aligned with a maximum $\theta = 35°$ to RD, cracking deflection may occur by cleavage in stage IV as shown in Fig. 16. It should be stated that, Fig. 16 delivers the typical cracking mechanisms of ZnAlMg coatings; however, an individual crack may also form in a zinc grain with unfavorable orientation without prior nucleation in the binary eutectic.

Considering the foundation laid in this study, some practical insights can be derived for reducing cracking tendency and accordingly designing a new generation microstructure controlled formable ZnAlMg coatings. The volume fraction of hard but brittle $MgZn_2$ intermetallic need to be reduced in the microstructure. This can be achieved by decreasing the fraction of binary eutectic encompassing large amount of $MgZn_2$ platelets. This solution is feasible by tailoring the composition (Al/Mg contents) in the coating and/or galvanization processing parameters. Orientation modification strategies should be implemented in such a way that (1) zinc grains orientate their basal plane parallel to the substrate/coating surface (Fig. 17a); (2) the basal plane of zinc grains preferably align parallel to tensile loading direction (Fig. 17b). In addition, grain refinement can be considered as a suitable solution to increase the ductility index by introducing more grain boundary and dislocation obstacles to resist crack propagation. This solution can be performed *via* composition control and/or modification of HDG process parameters.

5. Conclusions

The origin and mechanism of damage/cracking in hot-dip ZnAlMg coatings on a steel substrate is extensively investigated. Multi-aspect characterization and mechanical testing evaluations including nanoindentation coupled with EBSD, *in-situ* SEM tensile/bending, *in-situ* EBSD, μ-DIC analysis and XFEM simulations, are integrated to correlate the micro-mechanical properties with the microstructure in order to profoundly comprehend the cracking behavior. On the light of this study, corresponding microstructure controlled formable ZnAlMg coatings can be designed. The following conclusions can be summarized:

- The microstructure of Zn1.8Al1.8Mg coating consists of three typical constituents including primary zinc, binary eutectic and ternary eutectic. The binary eutectic contains zinc and $MgZn_2$ platelets whereas the ternary eutectic is composed of zinc, $MgZn_2$ and aluminum.
- According to the nanoindenation results, despite possessing the highest yield strength, the binary eutectic exhibits the lowest strain hardening exponent (n), *i.e.* the lowest micro-ductility among the phases. An empirical equation is proposed to correlate n with the orientation of the primary zinc grains to analyze the cracking tendency of individual grains.
- Based on the chronological observations during *in-situ* tests, most of the cracks are nucleated in the binary eutectic at hard but brittle $MgZn_2$ intermetallic platelets.
- μ-DIC and XFEM analyses reveal a substantial heterogeneous deformation leading to stress/strain localization mostly in the binary eutectic where most of the cracks initiate. In contrast, the ternary eutectic can bear large deformation without cracking.
- *In-situ* EBSD suggested that, compatible plastic deformation cannot be fulfilled in ZnAlMg coating and alternative twining mechanisms activate to accommodate imposed plastic deformation in zinc grains. The primary Zn grains with a small Schmid factor, twin boundaries and the binary eutectic phase/interface are detected as the most probable damage incident sites within the coating microstructure.
- Plastic deformation based criteria are revealed to explain/understand the cracking mechanism of the coating. In general, the primary Zn grains with a low Schmid factor ($m < 0.32$) and a low local strain hardening exponent ($n < 0.33$) as a result of their spatial orientation and mechanical anisotropy experience high cracking tendency during deformation.

CRediT authorship contribution statement

Masoud Ahmadi: Conceptualization, Investigation, Formal analysis, Writing - original draft. **Bekir Salgın:** Resources, Writing - review & editing. **Bart J. Kooi:** Formal analysis, Writing - review & editing, Supervision. **Yutao Pei:** Conceptualization, Formal analysis, Writing - review & editing, Supervision.

Declaration of competing interest

The authors declare that they have no known competing financial interests or personal relationships that could have appeared to influence the work reported in this paper.

Acknowledgement

Appendix A. Supplementary data

Supplementary data to this article can be found online at https://doi.org/10.1016/j.matdes.2019.108364.

References

[1] M. Van Schaik, C. Dane, B. Berkhout, MagiZinc-the new high performance coating for steel in the BIW and closures, SAE Technical Paper, 2016.
[2] N.C. Hosking, M.A. Ström, P.H. Shipway, C.D. Rudd, Corrosion resistance of zinc-magnesium coated steel, Corros. Sci. 49 (2007) 3669–3695, https://doi.org/10.1016/j.corsci.2007.03.032.
[3] E. De Bruycker, Z. Zermout, B.C. De Cooman, Zn-Al-Mg coatings: thermodynamic analysis and microstructure related properties, Mater. Sci. Forum 539–543 (2007) 1276–1281, https://doi.org/10.4028/www.scientific.net/MSF.539-543.1276.
[4] M. Kollárová, L. Hrabčáková, J. Graban, M. Šohajová, Structural properties of zinc and ZnMgAl coatings on steel sheets, Mater. Sci. Forum 782 (2014) 623–626, https://doi.org/10.4028/www.scientific.net/MSF.782.623.
[5] Y. Xie, A. Du, X. Zhao, R. Ma, Y. Fan, X. Cao, Effect of Mg on Fe–Al interface structure of hot–dip galvanized Zn–Al–Mg alloy coatings, Surf. Coatings Technol. 337 (2018) 313–320, https://doi.org/10.1016/j.surfcoat.2018.01.038.
[6] A. Dong, B. Li, Y. Lu, G. Zhu, H. Xing, D. Shu, B. Sun, J. Wang, Effect of Mg on the microstructure and corrosion resistance of the continuously hot-dip galvanizing Zn-Mg coating, Materials (Basel) 10 (2017) 980, https://doi.org/10.3390/ma10080980.
[7] N. Wint, N. Cooze, J.R. Searle, J.H. Sullivan, G. Williams, H.N. McMurray, G. Luckeneder, C. Riener, The effect of microstructural refinement on the localized corrosion of model Zn-Al-Mg alloy coatings on steel, J. Electrochem. Soc. 166 (2019) C3147–C3158.
[8] Y. Meng, G. Jiang, X. Ju, J. Hao, TEM study on the microstructure of the Zn-Al-Mg alloy, Mater. Charact. 129 (2017) 336–343, https://doi.org/10.1016/j.matchar.2017.05.011.
[9] M. Dutta, A.K. Halder, S.B. Singh, Morphology and properties of hot dip Zn-Mg and Zn-Mg-Al alloy coatings on steel sheet, Surf. Coatings Technol. 205 (2010) 2578–2584, https://doi.org/10.1016/j.surfcoat.2010.10.006.
[10] H.R. Bakhsheshi-Rad, E. Hamzah, H.T. Low, M. Kasiri-Asgarani, S. Farahany, E. Akbari, M.H. Cho, Fabrication of biodegradable Zn-Al-Mg alloy: mechanical properties, corrosion behavior, cytotoxicity and antibacterial activities, Mater. Sci. Eng. C. 73 (2017) 215–219, https://doi.org/10.1016/j.msec.2016.11.138.
[11] H. Asgari, M.R. Toroghinejad, M.A. Golozar, Effect of coating thickness on modifying the texture and corrosion performance of hot-dip galvanized coatings, Curr. Appl. Phys. 9 (2009) 59–66, https://doi.org/10.1016/j.cap.2007.10.090.
[12] M. Safaeirad, M.R. Toroghinejad, F. Ashrafizadeh, Effect of microstructure and texture on formability and mechanical properties of hot-dip galvanized steel sheets, J. Mater. Process. Technol. 196 (2008) 205–212, https://doi.org/10.1016/j.jmatprotec.2007.05.035.
[13] G. Vincent, N. Bonasso, J.S. Lecomte, B. Colinet, B. Gay, C. Esling, The relationship between the fracture toughness and grain boundary characteristics in hot-dip galvanized zinc coatings, J. Mater. Sci. 41 (2006) 5966–5975, https://doi.org/10.1007/s10853-006-0274-6.
[14] C.M. Wichern, B.C. De Cooman, C.J. Van Tyne, Surface roughness changes on a hot-dipped galvanized sheet steel during deformation at low strain levels, Acta Mater. 52 (2004) 1211–1222, https://doi.org/10.1016/j.actamat.2003.11.005.
[15] J.T.M. De Hosson, N. van der Pers, W.G. Sloof, G.M. Song, T. Vystavel, Relation between microstructure and adhesion of hot dip galvanized zinc coatings on dual

15

phase steel, Acta Mater. 60 (2012) 2973–2981, https://doi.org/10.1016/j.actamat.2012.02.003.

[16] G.M. Song, J.T.M. De Hosson, W.G. Sloof, Y.T. Pei, Evaluation of interface adhesion of hot-dipped zinc coating on TRIP steel with tensile testing and finite element calculation, WIT, Trans. Eng. Sci. 91 (2015) 3–14.

[17] R. Parisot, S. Forest, A. Pineau, F. Grillon, X. Demonet, J.M. Mataigne, Deformation and damage mechanisms of zinc coatings on hot-dip galvanized steel sheets: part I. Deformation modes, Metall. Mater. Trans. A Phys. Metall. Mater. Sci. 35 (A) (2004) 797–811, https://doi.org/10.1007/s11661-004-0007-x.

[18] R. Sagl, A. Jarosik, G. Angeli, T. Haunschmied, G. Hesser, D. Stifter, Tailoring of oxide morphology and crystallinity on advanced high-strength steel surfaces prior hot-dip galvanizing, Acta Mater. 72 (2014) 192–199, https://doi.org/10.1016/j.actamat.2014.03.037.

[19] R. Parisot, S. Forest, A.-F. Gourgues, A. Pineau, D. Mareuse, Modeling the mechanical behavior of a multicrystalline zinc coating on a hot-dip galvanized steel sheet, Comput. Mater. Sci. 19 (2000) 189–204, https://doi.org/10.1016/S0927-0256(00)00155-5.

[20] A.R. Marder, The metallurgy of zinc-coated steel, Prog. Mater. Sci. 45 (2000) 191–271.

[21] S.M.A. Shibli, B.N. Meena, R. Remya, A review on recent approaches in the field of hot dip zinc galvanizing process, Surf. Coatings Technol. 262 (2015) 210–215, https://doi.org/10.1016/j.surfcoat.2014.12.054.

[22] Z. Wu, S. Sandlöbes, L. Wu, W. Hu, G. Gottstein, S. Korte-Kerzel, Mechanical behaviour of Zn-Al-Cu-Mg alloys: deformation mechanisms of as-cast microstructures, Mater. Sci. Eng. A 651 (2016) 675–687, https://doi.org/10.1016/j.msea.2015.11.020.

[23] Z. Wu, S. Sandlöbes, J. Rao, J.S.K.L. Gibson, B. Berkels, S. Korte-Kerzel, Local mechanical properties and plasticity mechanisms in a Zn-Al eutectic alloy, Mater. Des. 157 (2018) 337–350, https://doi.org/10.1016/j.matdes.2018.07.051.

[24] Y.B. Park, I.G. Kim, S.G. Kim, W.T. Kim, T.C. Kim, M.S. Oh, J.S. Kim, Orientation dependence of cracking in hot-dip Zn-Al-Mg alloy coatings on a sheet steel, Metall. Mater. Trans. A Phys. Metall. Mater. Sci. 48 (2017) 1013–1020, https://doi.org/10.1007/s11661-016-3947-z.

[25] M. Dao, N. Chollacoop, K.J. Van Vliet, T.A. Venkatesh, S. Suresh, Computational modeling of the forward and reverse problems in instrumented sharp indentation, Acta Mater. 49 (2001) 3899–3918, https://doi.org/10.1016/S1359-6454(01)00295-6.

[26] K.C. Yu, J. Li, X. Liu, J.G. Li, X.H. Xue, Microstructure of hot-dip galvanized Zn-Al-Mg alloy coating, J. Shanghai Jiaotong Univ. 17 (2012) 663–667, https://doi.org/10.1007/s12204-012-1342-5.

[27] G.-R. Jiang, L.-F. Chen, H.-Q. Wang, G.-H. Liu, Microstructure and corrosion resistance property of a Zn-Al-Mg alloy with different solidification processes, MATEC Web Conf. 109 (2017) 0–4, https://doi.org/10.1051/matecconf/201710901004.

[28] S. Jakob, A. Leitner, A. Lorich, M. Eidenberger-Schober, W. Knabl, R. Pippan, H. Clemens, V. Maier-Kiener, Influence of crystal orientation and Berkovich tip rotation on the mechanical characterization of grain boundaries in molybdenum, Mater. Des. 182 (2019), 107998.

[29] Y.T. Pei, G.M. Song, W.G. Sloof, J.T.M. De Hosson, A methodology to determine anisotropy effects in non-cubic coatings, Surf. Coatings Technol. 201 (2007) 6911–6916, https://doi.org/10.1016/j.surfcoat.2006.11.044.

[30] H. Zunko, A. Hackl, H. Antrekowitsch, R. Ebner, R. Brisberger, Investigation on cracking behaviour of new Zn-based coatings on sheet steel for hot dip galvanising, Proc. 0f EMC 2009. Eur. Metall. Conf. 2009 2009, pp. 1534–1536 , Innsbruck, Ger.

[31] Y.B. Das, A.N. Forsey, T.H. Simm, K.M. Perkins, M.E. Fitzpatrick, S. Gungor, R.J. Moat, In situ observation of strain and phase transformation in plastically deformed 301 austenitic stainless steel, Mater. Des. 112 (2016) 107–116.

[32] R. Parisot, S. Forest, A. Pineau, F. Grillon, X. Demonet, J.-M. Mataigne, Deformation and damage mechanisms of zinc coatings on hot-dip galvanized steel sheets: part II. Damage modes, Metall. Mater. Trans. A. 35 (2004) 813–823.

[33] C. Tomé, U.F. Kocks, The yield surface of hcp crystals, Acta Metall. 33 (1985) 603–621.

[34] C. Niederberger, J. Michler, A. Jacot, Origin of intragranular crystallographic misorientations in hot-dip Al-Zn-Si coatings, Acta Mater. 56 (2008) 4002–4011, https://doi.org/10.1016/j.actamat.2008.04.037.

[35] T. Guo, L. Qiao, X. Pang, A.A. Volinsky, Brittle film-induced cracking of ductile substrates, Acta Mater. 99 (2015) 273–280.

[36] M. Ahmadi, B. Mohammad Sadeghi, H. Arabi, Experimental and numerical investigation of V-bent anisotropic 304L SS sheet with spring-forward considering deformation-induced martensitic transformation, Mater. Des. 123 (2017) 211–222, https://doi.org/10.1016/j.matdes.2017.03.040.

[37] G.M. Hughes, G.E. Smith, P.E.J. Flewitt, A.G. Crocker, The brittle fracture of polycrystalline zinc, Proc. R. Soc. A Math. Phys. Eng. Sci. 463 (2007) 2129–2151, https://doi.org/10.1098/rspa.2007.1866.

[38] P. Wen, M. Voshage, L. Jauer, Y. Chen, Y. Qin, R. Poprawe, J.H. Schleifenbaum, Laser additive manufacturing of Zn metal parts for biodegradable applications: processing, formation quality and mechanical properties, Mater. Des. 155 (2018) 36–45.